Low-cost fiber Bragg grating interrogation with a femtosecond laser written scattering chip

Przemyslaw Falak[a], Qi Sun[a], Tom Vettenburg[b], Timothy Lee[a], David B. Phillips[c], Gilberto Brambilla[a], and Martynas Beresna[a]

[a]University of Southampton, Southampton, SO17 1BJ, United Kingdom
[b]University of Dundee, Nethergate, Dundee, DD1 4HN, United Kingdom
[c]University of Exeter, Exeter, EX4 4QL, United Kingdom

ABSTRACT

Fiber Bragg gratings are the most popular type of optical fiber sensor. However, its commercial use is frequently limited by high cost and complexity of the interrogation unit. Here, an interrogator based on a femtosecond laser written silica scattering chip is designed and implemented. Such device can directly reconstruct strain, from the scattering speckle patterns, with a resolution of 70 $\mu\epsilon$ (microstrain) within the range of 180-700 $\mu\epsilon$, limited by the slippage of the fiber coating, with the potential to be reduced with the system improvements.

Keywords: scattering medium, FBG interrogator, speckle pattern, femtosecond laser writing, microstrain detection, fiber Bragg grating, strain sensing

1. INTRODUCTION

Fiber Bragg grating (FBG) devices and sensors can be found in many industries, including medicine, civil engineering, aeronautics, or telecommunications, owing to their mature and reliable fabrication technique, high responsivity, simple multiplexing and resistance to electromagnetic field interference. However, wider spread of FBGs is hampered by high cost and complexity of the interrogation units.[1] Due to the high sensitivity requirements for FBG-based sensors, the interrogation unit needs to trace fine-resolution spectral responses linked to the sensed quantity (spectral shift induced by strain, bending, pressure, temperature etc.)[2,3]

In order to achieve the desired performance, the devices are often expensive and complex, since realizing high spectral resolution for FBG interrogation requires micro-optics machining and high-precision engineering. Naturally, there is a trend to miniaturize and simplify the interrogators by inscribing them within waveguides, optical fibers or other photonics-integrated systems.[4–7] However, there are still challenges: manufacturing complexity, minimal traceable resolution and long-term stability. All the aforementioned systems were based on direct measurement of the optical response from the FBG. Here, we demonstrate an FBG interrogator system based on practical application of the spectral-to-spatial mapping approach.

The core principle of our approach utilizes a scattering medium as a spatial-spectral converter which generates unique and highly deterministic speckle patterns for different wavelengths.[8–10] Since applied strain will shift the FBG signal wavelength, this results in different speckle patterns. This in turn allows the system to directly reconstruct the strain values from the speckles, without needing to infer the spectral information. The interrogator itself is composed of only three elements: the scattering chip, collimator lens, and CMOS array (detector), assembled with Raspberry Pi platform for control. This is the first time a scattering chip reconstructive system acting as an FBG interrogator capable of detecting strain has been demonstrated.

2. DESIGN AND FABRICATION

2.1 Scattering chip

The scattering chip is made of 40 planes of femtosecond laser-written nanovoids separated 5 µm apart in the z direction (Fig. 1). Using multiple planes increases scattering efficiency by facilitating multiple backwards

Further author information: (Send correspondence to P.F.)
P.F.: E-mail: plf1n15@soton.ac.uk

and forward light passes (circa 60% of incident light was scattered).[11] Each plane measures 1 × 1 mm with 1000 × 1000 voids (average lateral void separation 1 µm). To enhance randomization of the wavefront, the position of each void was randomized in either the horizontal x or vertical y directions by adding an offset in range ±0.4 µm, alternating direction for each layer.[8] This design was a result of a trade-off between the total writing time and scattering efficiency of the chip. The fabrication time was 5 min per layer, resulting 200 min in total. To minimize impact of the environment (fluctuating temperature and humidity), high purity fused silica (UVFS C7980 0F) with low thermal expansion and OH content of 800-1000 ppm was selected as the substrate.[12]

Voids were formed by focusing into the substrate $\lambda = 515$ nm wavelength pulses generated as the second harmonic from a $\lambda = 1.03$ µm femtosecond laser system (PHAROS, Light Conversion Ltd., Lithuania) with 200 kHz repetition rate and 200 fs pulse duration. A 1.25 NA oil-immersion focusing objective was used on a z stage, with the substrate (10 × 10 × 1 mm) on an x-y stage for translation perpendicular to the writing beam direction. An overhead CMOS camera allowed visual inspection of the written structure in-situ.

2.2 Enclosure assembly

Since the assembled FBG interrogator parts are delicate and its working principle requires these to be shielded from ambient light, the 3D printed enclosure was designed to minimize device footprint, maximize stability

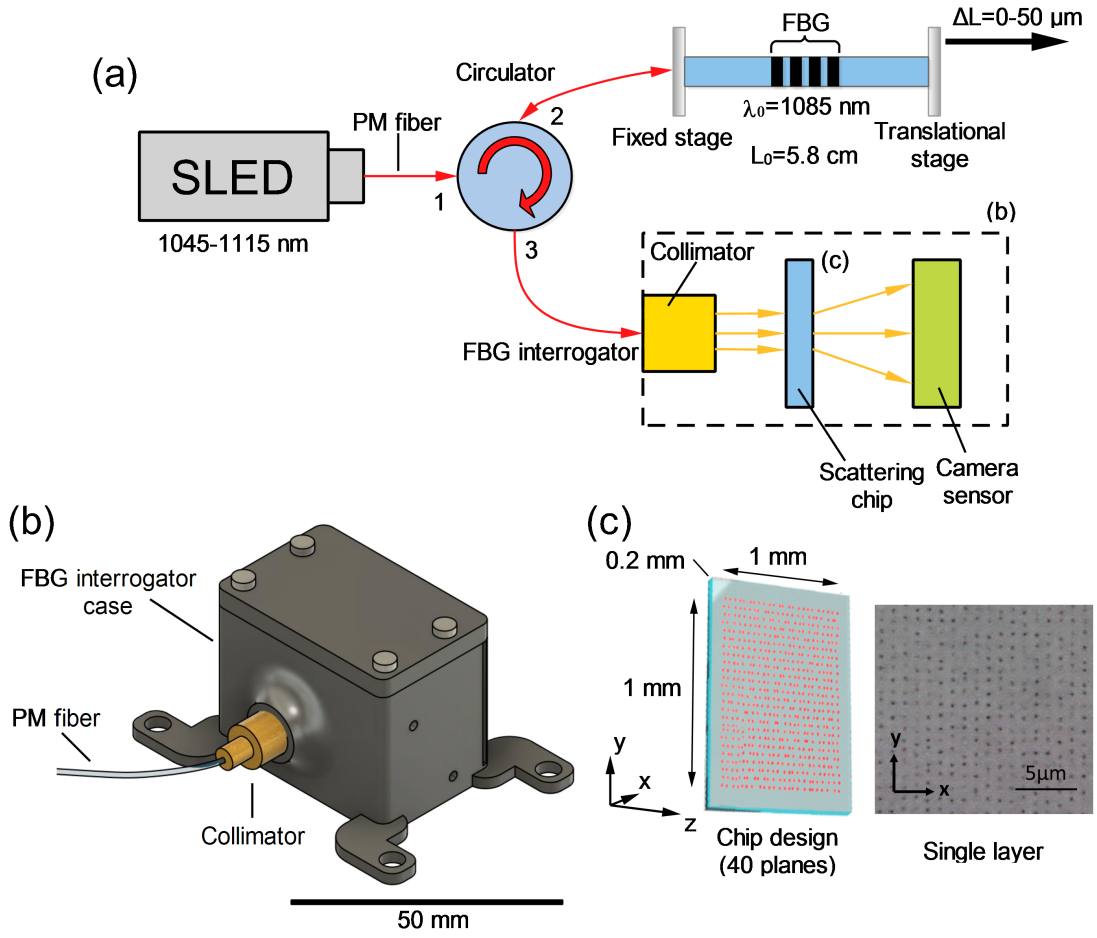

Figure 1. (a) Experimental set-up for FBG interrogation, (b) interrogator body, (c) scattering chip design and microscope image of a single plane of voids. Note: numbers by the circulator symbol in (a) indicate its ports 1, 2 and 3.

(protection from fluctuating environmental conditions and ambient light) as well as mechanically protect delicate electronic parts.

The box was printed from Tough PLA (Ultimaker) with dimensions of 57 × 35 × 35 mm (Fig. 1b), and includes a holder for fixing the detector (CMOS array), placement for the scattering medium, an input signal collimator, mounting space and a removable top cover for access.

3. METHOD OF OPERATION

3.1 Experimental set up

The FBG interrogator operates on the two phenomena: the Bragg resonance wavelength's strain dependence and spatial-to-spectral mapping. By applying tensile strain, the reflected Bragg wavelength shifts towards higher values. This reflected light is launched into the scattering medium (chip), and since each wavelength component produces unique and highly-deterministic speckle patterns, an unknown strain value can be recovered from the captured speckles.[10,13]

Initial calibration is performed by recording FBG-reflected speckle patterns for different strain values. Next, during measurement for an unknown given strain (known to be within the range of calibration values), the system captures the speckle pattern and finds the correlation factors between the measured and each of the previously obtained calibration reference patterns. The highest correlation factor indicates which reference pattern correspond most with the measured one, and hence identifying the measured strain.[14]

The experimental set-up for both calibration and measurement are the same (Fig. 1a): a superluminescent LED (SLED) source with a 70 nm bandwidth and a central wavelength of 1080 nm (SLD-1080-30-PM-100, Innolume) was connected via the polarization-maintaining fiber (PM) to the optical circulator via port 1 (input).

The in-house laser-written FBG for strain measurement had an unstrained reflection peak at 1085.016 nm and 0.17 nm linewidth (Figure 2a), with a length of 3 mm. The FBG was attached to the port 2 of the optical circulator. To induce the strain, the 5.8 cm section of FBG fiber was mounted on two translational stages (MAX381, Thorlabs). During measurements, one stage remained fixed while the other was displaced in the range from 0 to 50 μm with 0.5 μm increments, which corresponds to a microstrain ($\mu\epsilon$) range from 0 to 850 $\mu\epsilon$ with a step of 20 $\mu\epsilon$. The reflected signal re-enters the circulator at port 2 and leaves the device from port 3 towards the demonstrated FBG interrogator, where the light is scattered by the chip and mapped to the speckle pattern. The speckle patterns were captured via the detector as a 640 × 480 pixel image (single pixel size of 1.12 × 1.12 μm). Such resolution was selected as a good balance between speckle visibility and computational speed.

3.2 Strain measurement

To measure the strain values, each speckle pattern image was vectorized - reshaped into column vector by stacking each consecutive column of the speckle on the bottom of the previous one. The resulting speckle vector S_v has 307200 pixels elements (total of a 640 × 480 pixels speckle pattern). By comparing the measured data $M(S_v, r)$ against the calibrated (reference) dataset $C(S_v, \mu\epsilon)$ the strain information can be revealed.[15] The calibration data contains vectorized speckles obtained during calibration for individual strains ($\mu\epsilon$). The measured data structure is similar, yet it contains only r speckle patterns collected during measurement. By using Eq. (1) the correlation coefficient vector $R_{\mu\epsilon}$ can be evaluated between each test and calibration speckle patterns. Therefore, by finding the highest correlation coefficient, the most probable strain for the measured data can be identified. Therefore, such system can work either as the FBG interrogator (strain sensing), but also as a spectrometer, since the speckle patterns are wavelength dependent.[8,9]

$$M(S_v, r) = C(S_v, \mu\epsilon) * R_{\mu\epsilon} \tag{1}$$

Since the Eq. (1) represents the linear set of equations it can be written more succinctly as a matrix equation: $M = CR_{\mu\epsilon}$. If the noise-free measurement can be presumed, the strain coefficients vector $R_{\mu\epsilon}$ can be obtained from the following relation: $R_{\mu\epsilon} = C^{-1}M$. Whilst it may seem trivial to solve this equation, the inverse of a non-square matrix is non-existent (which is true for almost all the cases, since total number of single-speckle pixels

is much greater than the number of captured speckles). The solution to this computation problem is to use the Moore-Penrose pseudo-inverse of the matrix C, which can be calculated from the singular value decomposition: $C = U\Sigma V^T$ as $C^{-1} = V\Sigma^{-1}U^T$.[16–18] U and V are unitary matrices, Σ is a diagonal matrix with the singular values and ^{T} denotes the matrix transpose. Matrix Σ^{-1} is obtained by reciprocating the main diagonal of the Σ matrix (singular values) and then transposing the resulted matrix.

4. RESULTS AND DISCUSSION

4.1 FBG response linearity

Before the actual device-based interrogation can take place, the linearity of response from the investigated FBG was checked by replacing the interrogator with a commercial optical spectral analyzer (Yokogawa AQ6370D), as shown in Figure 1a. Then, the translational stage was moved to induce tensile strain in the range 0-50 µm with 0.5 µm steps. Simultaneously, the shift of the reflected Bragg wavelength peak was tracked.

The relative wavelength shift and the strain are related by the following equations (Equation 2 and 3):

$$\epsilon = \frac{L - L_0}{L_0} = \frac{\Delta L}{L_0} \tag{2}$$

$$\frac{\lambda - \lambda_0}{\lambda_0} = \frac{\Delta\lambda}{\lambda_0} = \kappa\epsilon \tag{3}$$

Where: L - fiber length with applied strain; L_0 - initial FBG fiber length (no strain applied); ΔL - fiber length change as an effect of strain applied; λ - peak position of the reflected Bragg wavelength with strain applied; λ_0 - initial FBG reflection peak (no strain applied); $\Delta\lambda$ - Bragg reflection wavelength shift; κ - linearity coefficient, dependent on elasto-optic properties and extension of the grating.

It is important to note that due to the 'slippage effect' - relative displacement or shear between the polymer coating and the fiber cladding, as well as with the translational stage holder magnets, two kinds of strain are in fact present: the recorded strain which relates to that applied to the fiber outer layer (polymer), and the internal FBG strain experienced by the core. As a consequence, for a given displacement of the translational stage, the polymer coating would displace more than the core itself. Hence the values of the linearity coefficient κ from Equation 3 would be lower for the measured system than expected from literature.[13]

For the investigated FBG, the linearity parameter κ can be obtained from the measurements trend line (Figure 2b). The experimental value of the coefficient is smaller than expected (0.497 vs 0.79), which indeed

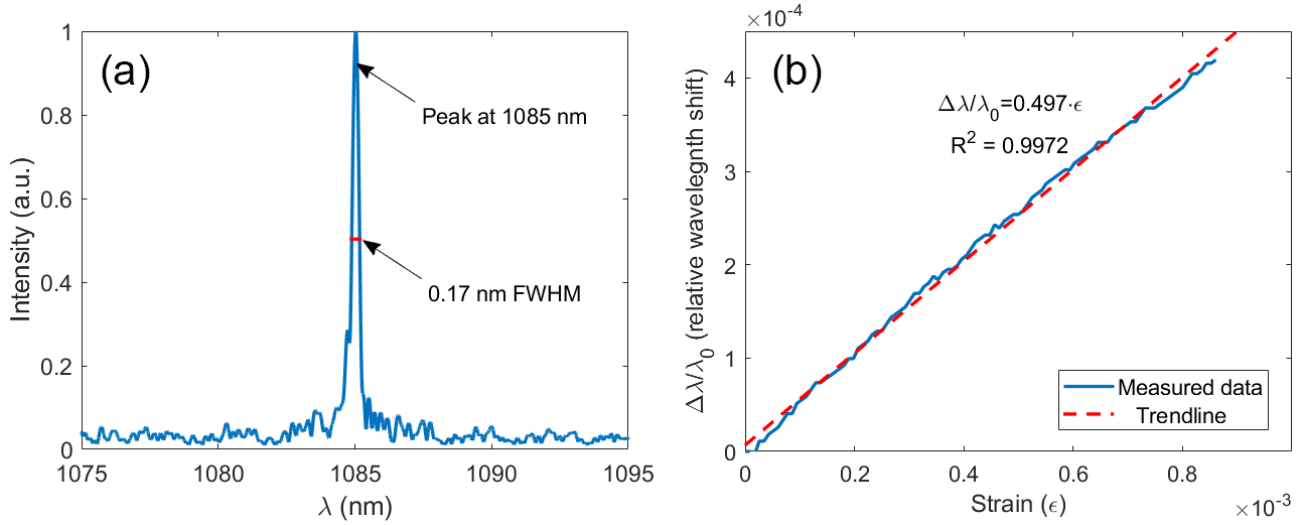

Figure 2. Investigated FBG: (a) reflection spectrum (no strain applied); (b) response linearity: relative wavelength shift as a function of strain. The linear coefficient equals 0.497.

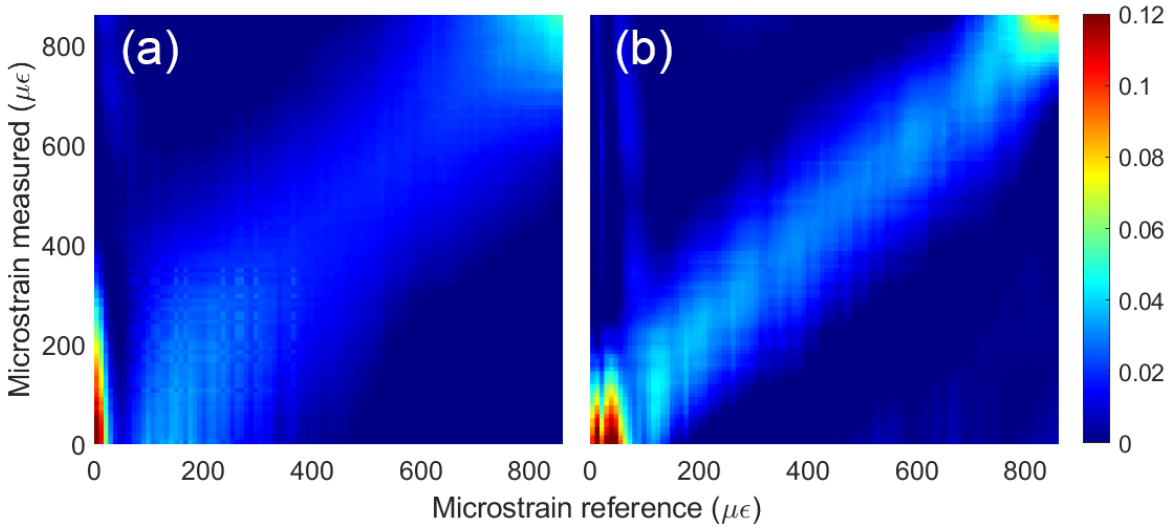

Figure 3. Correlation matrices for: (a) scattering chip-based device; (b) 50 cm straight MMF. Colorbar scale refers to correlation coefficient values.

confirms the slippage effect impact on the strain measurements. Overall, the linearity of the wavelength shift from the investigated FBG under tensile strain has been confirmed, but the 'slippage effect' shall be considered as a potential challenge.

4.2 Strain measurement: scattering chip vs. MMF (multi-moded fiber)

Since the linear response of the FBG has been confirmed, the scattering chip-based device was tested as the interrogator. To cross-compare its capabilities, a 50 cm MMF section (FG105LCA, Thorlabs) mounted on a straight guide rail was selected as a representative scattering medium for comparison. The correlation matrices - relations between speckles for the same strain range for both calibration and testing sequences in the ideal scenario would have high intensity main diagonal values and low noise values elsewhere.[14] The correlation results for both the chip and MMF are presented in Figure 3.

Both results exhibit similar behaviour: the main diagonal does exist, but it is wider than expected from the theory and its intensity is very low, which can be quantified by the signal-to-noise ratio - it equals only 3 for chip and 2 for the MMF-based system. Moreover, the correlation noticeably increases in both low (0-180 $\mu\epsilon$) and high (700-850 $\mu\epsilon$) strain value regions, which can be explained by previously discussed (section 4.1) 'slippage effect': the internal strain remained unchanged, or very low when the external applied strain is initially increased. Once the strain value is high enough, the reconstruction improves, but the slippage still causes the diagonal to blur. Finally, at the highest strain ranges, the correlation increases again, which can be interpreted as the inability to induce strain onto the fiber due to the slippage between stages and fiber as well as the polymer coating and the cladding (similar effect to the one with minimal strain applied).

Despite the scattering chip-based device diagonal being more blurred (hence worse reconstruction of the strain values) than the MMF, one significant advantage can be observed: the off-diagonal correlation, which represents the background noise level, is higher for the MMF than for the chip (0.035 vs. 0.018), which implies worse stability from the fiber-based system even over the short-term (total measurement time was only 650 s). Such medium demonstrates excellent resolution, but is known to suffer from poor temporal stability.[19] For a long-term reconstruction, the chip-based device would be superior, since its high temporal stability was already demonstrated.[8,9]

To quantify the devices' performance, the strain values were reconstructed using the highest correlation value for the given strain reference (column-wise) from their correlation matrices as shown in Figure 4. For each test, the applied strain was increased linearly from 0 to 850 $\mu\epsilon$ over the time span shown. The results confirm the previous findings: over the sensing range 180-700 $\mu\epsilon$, the strain reconstruction can be applied successfully with a

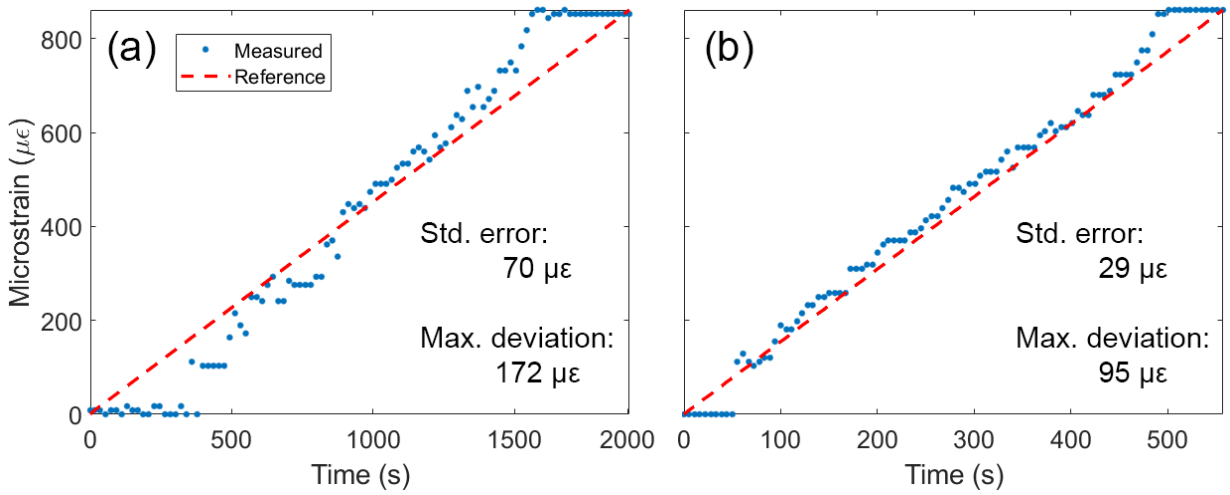

Figure 4. Tensile microstrain reconstruction: (a) scattering chip-based device; (b) 50 cm MMF. This figure shall be read in conjunction with the Figure 3. In both tests, the applied strain is ramped linearly from 0 to 850 $\mu\epsilon$ over the time span shown.

linear response. Outside of this range, the reconstructive capability is limited by the slippage effect. Interestingly, the usable sensing strain range is the same for both the MMF and scattering chip system, implying that it is independent of the device used and is purely linked to the FBG slippage on the testing stages.

However, the quality of the reconstruction in the sensing range clearly depends on the utilized medium. Although both reconstructions (Figure 4) are linear, the scattering chip reconstruction is slightly tilted relative to the reference strain, whilst the MMF maintains the same gradient as the reference at all times in the sensing range. To quantify the reconstructions, the standard error and maximum deviation values were calculated. Indeed, the demonstrated chip-based device can reconstruct the strain with the standard error equal to 70 $\mu\epsilon$ and the maximum deviation of 172 $\mu\epsilon$ and for the MMF-based system, these numbers were reduced to 29 and 95 $\mu\epsilon$ accordingly (including the slippage effect).

5. CONCLUSION

We demonstrated a highly stable, compact, and low cost FBG interrogator based on a tailored femtosecond laser-written scattering medium, in which the FBG back-reflected light is used to generate speckle patterns. By calibrating different FBG strain to their corresponding speckle patterns, an unknown test strain can be reconstructed via a singular value decomposition technique.

The device was capable of reconstructing applied strain in the range 180-700 $\mu\epsilon$ with 70 $\mu\epsilon$ resolution (standard reconstruction error). Over this range, the Bragg peak wavelength varies from 1085.016 to 1085.467 nm, which corresponds to the spectral wavelength shift resolution of 0.06 nm. The limitations of the minimal and maximal traceable strain were due to the 'slippage effect' between the FBG fiber coating and the tensioning translation stages.

The comparison between the scattering chip-based device and an MMF-based system demonstrated the latter to achieve finer strain resolution (29 $\mu\epsilon$), whereas the former showed an improved correlation signal-to-noise ratio of 3 (compared with 2 for the MMF-based system) due to its superior temporal stability.

REFERENCES

[1] Casas-Ramos, M. A. and Sandoval-Romero, G. E., "Strain detection and measurement using a matched fibre Bragg grating," *J. Electromagn. Waves Appl.* **32**(12), 1519–1526 (2018).

[2] Qin, H., Tang, P., Lei, J., Chen, H., and Luo, B., "Investigation of strain-temperature cross-sensitivity of FBG strain sensors embedded onto different substrates," *Photonic Sens.* **13**(1), 230127 (2022).

[3] Ramly, R., Kuntjoro, W., and Rahman, M. K. A., "Using embedded fiber Bragg grating (FBG) sensors in smart aircraft structure materials," *Procedia Eng.* **41**, 600–606 (2012).

[4] Marin, Y. E., Nannipieri, T., Oton, C. J., and Pasquale, F. D., "Current status and future trends of photonic-integrated FBG interrogators," *J. Lightwave Technol.* **36**(4), 946–953 (2018).

[5] Ogawa, K., Koyama, S., Haseda, Y., Fujita, K., Ishizawa, H., and Fujimoto, K., "Wireless, portable fiber Bragg grating interrogation system employing optical edge filter," *Sensors* **19**(14), 3222 (2019).

[6] Li, Y., Lu, B., Ren, L., Chen, H., Qiu, Y., Mao, B., Zhou, P., Zhao, C., and Dong, X., "A highly precise FBG sensor interrogation system with wavemeter calibration," *Opt. Fiber Technol.* **48**, 207–212 (2019).

[7] Marrazzo, V. R., Fienga, F., Riccio, M., Irace, A., and Breglio, G., "Multichannel approach for arrayed waveguide grating-based FBG interrogation systems," *Sensors* **21**(18), 6214 (2021).

[8] Falak, P., Sun, Q., Vettenburg, T., Lee, T., Phillips, D. B., Brambilla, G., and Beresna, M., "Femtosecond laser written scattering chip for high-resolution low-cost reconstructive spectrometry," in [*Photonic Instrumentation Engineering IX*], **12008**, 120080E, International Society for Optics and Photonics, SPIE (2022).

[9] Sun, Q., Falak, P., Vettenburg, T., Lee, T., Phillips, D. B., Brambilla, G., and Beresna, M., "Compact nano-void spectrometer based on a stable engineered scattering system," *Photon. Res.* **10**(10), 2328–2336 (2022).

[10] Yang, Z., Albrow-Owen, T., Cai, W., and Hasan, T., "Miniaturization of optical spectrometers," *Science* **371**(6528), eabe0722 (2021).

[11] Sun, Q., Vettenburg, T., Lee, T., Phillips, D., Beresna, M., and Brambilla, G., "Compact spectrometer chips based on fs laser written multi-layer scattering medium," *Asia Commun. Photonics Conf. ACP 2019* , T4D.5, Optical Society of America (2019).

[12] Drotning, W. D., "Thermal expansion of glasses in the solid and liquid phases," *Int. J. Thermophys.* **6**(6), 705–714 (1985).

[13] Campanella, C. E., Cuccovillo, A., Campanella, C., Yurt, A., and Passaro, V. M. N., "Fibre Bragg grating based strain sensors: Review of technology and applications," *Sensors* **18**(9), 3115 (2018).

[14] Redding, B., Popoff, S. M., Bromberg, Y., Choma, M. A., and Cao, H., "Noise analysis of spectrometers based on speckle pattern reconstruction," *Appl. Opt.* **53**(3), 410–417 (2014).

[15] Redding, B., Popoff, S. M., and Cao, H., "All-fiber spectrometer based on speckle pattern reconstruction," *Opt. Express* **21**(5), 6584–6600 (2013).

[16] Baksalary, O. M. and Trenkler, G., "The Moore–Penrose inverse: a hundred years on a frontline of physics research," *Eur. Phys. J. H* **46**(1), 9 (2021).

[17] Sadek, R. A., "SVD based image processing applications: State of the art, contributions and research challenges," *Int. J. Adv. Comput. Sci. Appl.* **3**(7) (2012).

[18] Brunton, S. and Kutz, J., "Singular value decomposition (SVD)," in [*Data-driven Science and Engineering: Machine Learning, Dynamical Systems, and Control*], 3–46, Cambridge University Press (2019).

[19] Redding, B., Alam, M., Seifert, M., and Cao, H., "High-resolution and broadband all-fiber spectrometers," *Optica* **1**(3), 175–180 (2014).